Basin Research (2008) doi: 10.1111/j.1365-2117.2008.00366.x

Pro- vs. retro-foreland basins

M. Naylor and H. D. Sinclair

School of GeoSciences, Grant Institute, University of Edinburgh, Edinburgh,UK

ABSTRACT

Alpine-type mountain belts formed by continental collision are characterised by a strong cross-sectional asymmetry driven by the dominant underthrusting of one plate beneath the other. Such mountain belts are flanked on either side by two peripheral foreland basins, one over the underthrust plate and one over the over-riding plate; these have been termed pro- and retro-foreland basins, respectively. Numerical modelling that incorporates suitable tectonic boundary conditions, and models orogenesis from growth to a steady-state form (i.e. where accretionary influx equals erosional outflux), predicts contrasting basin development to these two end-member basin types. Pro-foreland basins are characterised by: (1) Accelerating tectonic subsidence driven primarily by the translation of the basin fill towards the mountain belt at the convergence rate. (2) Stratigraphic onlap onto the cratonic margin at a rate at least equal to the plate convergence rate. (3) A basin infill that records the most recent development of the mountain belt with a preserved interval determined by the width of the basin divided by the convergence rate. In contrast, retro-foreland basins are relatively stable, are not translated into the mountain belt once steady-state is achieved, and are consequently characterised by: (1) A constant tectonic subsidence rate during growth of the thrust wedge, with zero tectonic subsidence during the steady-state phase (i.e. ongoing accretion–erosion, but constant load). (2) Relatively little stratigraphic onlap driven only by the growth of the retro-wedge. (3) A basin fill that records the entire growth phase of the mountain belt, but only a condensed representation of steady-state conditions. Examples of pro-foreland basins include the Appalachian foredeep, the west Taiwan foreland basin, the North Alpine Foreland Basin and the Ebro Basin (southern Pyrenees). Examples of retro-foreland basins include the South Westland Basin (Southern Alps, New Zealand), the Aquitaine Basin (northern Pyrenees), and the Po Basin (southern European Alps). We discuss how this new insight into the variability of collisional foreland basins can be used to better interpret mountain belt evolution and the hydrocarbon potential of these basins types.

INTRODUCTION

Foreland basins are the sedimentary basins located on continental lithosphere at the outer edge of mountain belts (cf. Dickinson, 1974). They are formed by the regional isostatic compensation by lithospheric flexure driven by both the topography and internal density variations of mountain ranges; additional bending forces on the down-flexed lithosphere may also drive further subsidence (for review see Beaumont, 1981; Jordan, 1981). Foreland basins are characterised by a regionally low gravity anomaly that broadly mimics the geometry of the flexural profile of the underlying lithosphere (Karner & Watts, 1983). This geometry also results in a marked asymmetry in cross-section of foreland basins, with a much deeper orogenic margin beneath the deformation front of the mountain belt, and a wedge-shaped form that tapers out over the stable cratonic margin of the basin (Allen *et al*., 1986). Their dimension perpendicular to the mountain front ranges from $100 < L_{\text{basin}} < 300$ km depending on the wavelength of isostatic compensation which is a function of the flexural rigidity of the lithosphere. The cratonic margin of foreland basins may be defined by the point of zero deflection that separates the downflexed basin from the region of forebulge uplift. This is best recorded by marine settings, where the palaeocoastline is used as a proxy for this point (Crampton & Allen, 1995). In continental basin fills, it is common for sediment to drape well beyond the point of zero deflection, and hence DeCelles & Giles (1996) advocated the use of 'forebulge' and 'backbulge depocenters'.

The first recognition of the variety of foreland basin types was by Dickinson (1974) who distinguished retro-arc from peripheral foreland basins. The former develops during ocean-continent collision associated with the growth of a magmatic arc. In this case, the foreland basin evolves on the continental side of the mountain belt as seen to the east of the Andes and the Rockies (Jordan, 1995). In contrast, peripheral foreland basins develop on both sides of a mountain belt resulting from continent–continent collision (for review see Miall, 1995); well-documented examples of peripheral foreland basins include the

Correspondence: M. Naylor, School of GeoSciences, Grant Institute, University of Edinburgh, West Mains Rd, Edinburgh EH9 3JW, UK. E-mail: mark.naylor@ed.ac.uk

North Alpine Foreland Basin of western Europe and the Ganges Basin of northern India.

Understanding differences in tectonic boundary conditions for peripheral foreland basin types came from the analysis of doubly vergent thrust wedges where one thrust wedge evolves over the underthrust lithosphere, and the opposing wedge develops over the overriding plate (Fig. 1) (Willett *et al*., 1993). Johnson & Beaumont (1995) used a numerical model to simulate the evolution of peripheral foreland basins on either side of a doubly vergent mountain belt. In so doing, they introduced the terms pro- and retro-foreland basins in order to distinguish the basin overlying the underthrust plate from that overlying the overriding plate, respectively (Fig. 1); we adopt this terminology for distinguishing between these peripheral foreland basin types. While the nominal distinction between pro- and retro-foreland basins on either side of a mountain belt has been recognised in terms of basin setting (e.g. Allen & Allen, 2005), no criteria in terms of basin evolution, subsidence histories or stratigraphic architecture have yet been provided to distinguish between them. This study focuses on distinguishing peripheral foreland basins using these criteria, but also highlights the potential significance for retro-arc basin types.

We use numerical modelling to investigate the stratigraphic record of peripheral foreland basins. The temporal evolution of these basins is divided into a growth phase where the topographic mass of the mountain belt increases and a steady state phase where the topographic mass remains constant (Willett & Brandon, 2002). The contrasting tectonic boundary conditions are explored for the side of a mountain belt experiencing active underthrusting and accretion (pro-side sensu Willett *et al*., 1993) vs. the side that is being overthrust, and which experiences relatively little accretion (retro-side sensu Willett *et al*., 1993, Fig. 1). By comparing results from these experiments with natural examples, we demonstrate the marked contrast between these basin types, and go on to provide new predictions for stratal architecture, chronostratigraphy and subsidence that discriminate between them. We conclude by exploring the implications for interpretations of tectonics from stratal records, and for hydrocarbon prospectivity.

Background on foreland basins

The primary criteria used to characterise the stratigraphic infill of foreland basins are thickness, lateral extent, rates of subsidence, rates of onlap and broad depositional environments. Numerical models that combine the tectonics of the system with algorithms to simulate surface processes have been used to analyse basin development and predict

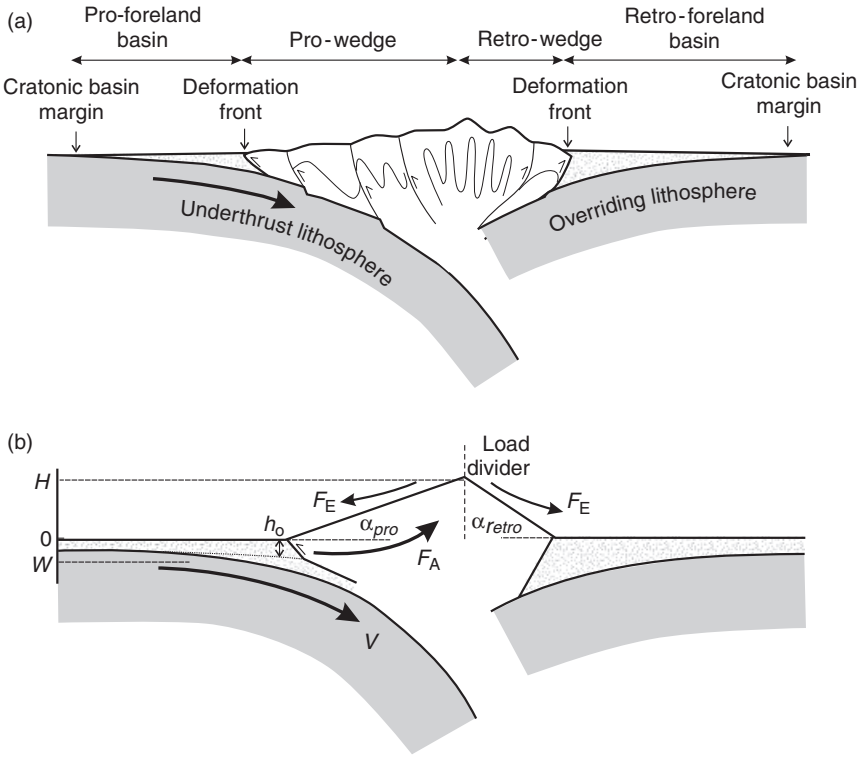

Fig. 1. Cartoon of a steady-state doubly vergent orogen. (a) The pro-foreland basin lies in the flexural depression over the subducting slab which advances towards the orogen at the regional convergence rate, v. The retro-foreland basin lies in the flexural depression above the over-riding slab which is predominantly stationary with respect to the orogen. (b) The mass budget of the wedge system is controlled by the relative rate of the accretionary and erosive fluxes (F_A and F_E, respectively). The rate of accretion of new material from the downgoing plate is a function of the convergence rate and the thickness of material that is accreted from that plate, h_0. The cross-sectional area of the mountain's topography is described by two triangles of height H and surface taper angles α_{pro} and α_{retro} that abut at the load divider.

 Basin Research, 10.1111/j.1365-2117.2008.00366.x

these characteristics for different boundary conditions and parameter sets. Initially, these models used blocks progressively added onto an elastic plate to simulate the progressive addition of thrust sheets into a wedge and their flexural response (Beaumont, 1981; Jordan, 1981; Quinlan & Beaumont, 1984). A significant advance was provided by a model that coupled the growth of a single, critically tapered thrust wedge to the infill of a foreland basin through the simulation of erosion and sedimentation by a diffusion algorithm (Flemings & Jordan, 1989; Sinclair *et al.*, 1991). A more sophisticated surface process model coupled to a doubly vergent thrust wedge model was used to explore the impact of the asymmetry of orographically enhanced precipitation over mountain ranges (Johnson & Beaumont, 1995). This important insight into the potential impact of orogenic asymmetry on the two neighbouring foreland basins hinted at the prospect of fundamental differences in basin types. Recent models of thrust wedge development have evolved to demonstrate the intimate coupling between the timescale of deformation on localised structures to the surface processes response time (Simpson, 2006); this has implications for the link between propagation of the deformation front, filling of the basin, and source areas for sediment.

Numerical model developments have evolved in parallel with improved documentation of a range of basins from around the world. Studies of peripheral foreland basins have been dominated by those developed on the pro-side of a mountain belt due to the improved access to surface exposures of foreland basin sediments that have been accreted and deformed within the thrust wedge. For example, the notion that subsidence in foreland basins should accelerate through time was initially tested in the North Alpine Foreland Basin (Allen *et al.*, 1986), and by subsequent analyses in the Ebro Basin of the Pyrenees (Vergés *et al.*, 1998) and in southeastern Papua New Guinea (Haddad & Watts, 1999). The erosion of a region of forebulge uplift was first documented and modelled from the Appalachian and North Alpine systems (Quinlan & Beaumont, 1984; Crampton & Allen, 1995). Comparisons have been made between the progressive stratigraphic onlap of the outer craton of foreland basins with the time-equivalent activity of the deformation front in the North Alpine and Himalayan systems (Homewood *et al.*, 1986; Burbank *et al.*, 1996; Sinclair, 1997). Finally, tectonostratigraphic models for the progressive evolution of 'peripheral' foreland basins from a deep-water 'underfilled' stage to a shallow marine to continental 'filled' or 'overfilled' stage have been provided by the Appalachian, Himalayan and North Alpine Foreland Basins (Stockmal *et al.*, 1986; Sinclair & Allen, 1992; Sinclair, 1997).

In contrast, retro-foreland basins have been relatively understudied, except where extensive subsurface data exists. Hence, basins like the Aquitaine Basin to the north of the Pyrenees, or the South Alpine foreland basin have had little impact on the development of stratigraphic models for peripheral foreland basins. We argue that our mechanical understanding of foreland basins is currently based on the model for pro-foreland basin types, but that this represents only half the story, lacking a comparative model for retro-foreland basins.

Here, we use a numerical model of a mountain belt whose asymmetry into pro- and retro-sides is defined by the asymmetry of underthrusting. We consider the impact of this asymmetry on the stratigraphic development of the opposing peripheral foreland basins, and so provide a new model aimed at distinguishing the subsidence and stratigraphic development of pro- vs. retro-foreland basins. The model only analyses the main foredeep of foreland basin systems (sensu DeCelles & Giles, 1996), we do not consider the impact upon wedge-top or forebulge sedimentation.

THE MODEL

We investigate the coupled evolution of the pro- and retro-foreland foreland basins (Fig. 1) that bound a collisional mountain belt. Because there are many regional special cases that can be considered, we choose a parameterisation that produces a singular solution which we believe reflects the most general case from which more complicated system-specific cases can be considered. The sensitivity of the model to varying the parameterisation is reserved until the 'Summary and Discussion' section.

The total system area, A_{system} above the flexed slabs is broken down into a topographic component A_{topo}, and the region bounded below the zero deflection datum and above the flexed slabs, A_{fill} which comprises the basin infill and the root of the mountain belt. We consider two phases of evolution of the system; (a) its growth phase, where the area of the topographic wedge is increasing $\frac{\mathrm{d}A_{\text{system}}}{\mathrm{d}t} > 0$ and (b) its subsequent steady-state phase, where the influx of material F_A into the topographic wedge is balanced by the erosional efflux F_E out of the wedge and $\frac{\mathrm{d}A_{\text{system}}}{\mathrm{d}t} = 0$. This transition occurs as the volume of a mountain belt increases, assuming a constant rate of accretion, because surface uplift rates progressively decrease, allowing uplift and erosion rates to converge (Dahlen & Suppe, 1988).

The model requires the integration of three components:

(1) A topographic model that describes the cross-sectional profile of the mountain belt from which the topographic load is derived.
(2) Tectonic boundary conditions that describe both the rate of accretion of new material into the system and the advection of the basins due to the motion of the underlying slabs.
(3) A flexural model for the semi-infinite slabs that respond to the topographic load.

Topographic model

The form of the mean topographic elevation of the doubly vergent mountain belt is approximated by two triangles of

the same height, H, abutting back to back (Fig. 2). Thus the total cross-sectional area of the topographic load is given by:

$$A_{\text{topo}} = \frac{H^2}{2\tan\alpha_{\text{pro}}} + \frac{H^2}{2\tan\alpha_{\text{retro}}} \quad (1)$$

Pro- and retro-wedges accrete material in kinematically different ways (Willett, 1992), which leads to a characteristically different topographic form. The pro-wedge grows by the accretion of material at the toe, which leads to the stress solution corresponding to the minimum taper angle predicted by critical wedge theory (Davis *et al.*, 1983; Dahlen *et al.*, 1984). However, the retro-wedge predominantly grows by material added at the back of the wedge and has the maximum taper angle predicted by critical wedge theory (Willett, 1992). We apply typical surface angles of $\alpha_{\text{pro}} = 1.5^\circ$, $\alpha_{\text{retro}} = 2.5^\circ$ which are at the lower end of typical wedge angles (e.g. Davis *et al.*, 1983; Ford, 2004) to highlight the impact of load distribution. Thus, the cross-sectional area of our modelled topography with the mean elevation at the highest point $H_{\max} = 3$ km is $A_{\text{topo}} = 275\,\text{km}^2$, generating a pro-wedge 115 km wide and a retro-wedge 69 km wide. This represents the maximum topographic load applied in this study.

Tectonic boundary conditions

The tectonic boundary conditions are the underlying source of asymmetry (Fig. 1b). The simulated mountain belt evolves above the subduction zone as a consequence of new material being accreted into the system from the down going plate. The slab underlying the pro-foreland basin is continually translated towards and down the subduction zone at the regional convergence rate. The pro-foreland stratigraphic model incorporates this by translating the basin fill along and down the subducting slab, creating new accommodation space. In contrast, the retro-foreland basin fill, on the overlying slab, is not translated toward the subduction zone. This study uses a convergence rate of $v = 5\,\text{km}\,\text{Myr}^{-1}$ typical to a number of settings (e.g. Beaumont *et al.*, 2000). This velocity represents the rate at which material is translated towards the mountain belt from the far field. Further, we simulate the case where the basins are instantaneously filled to the level

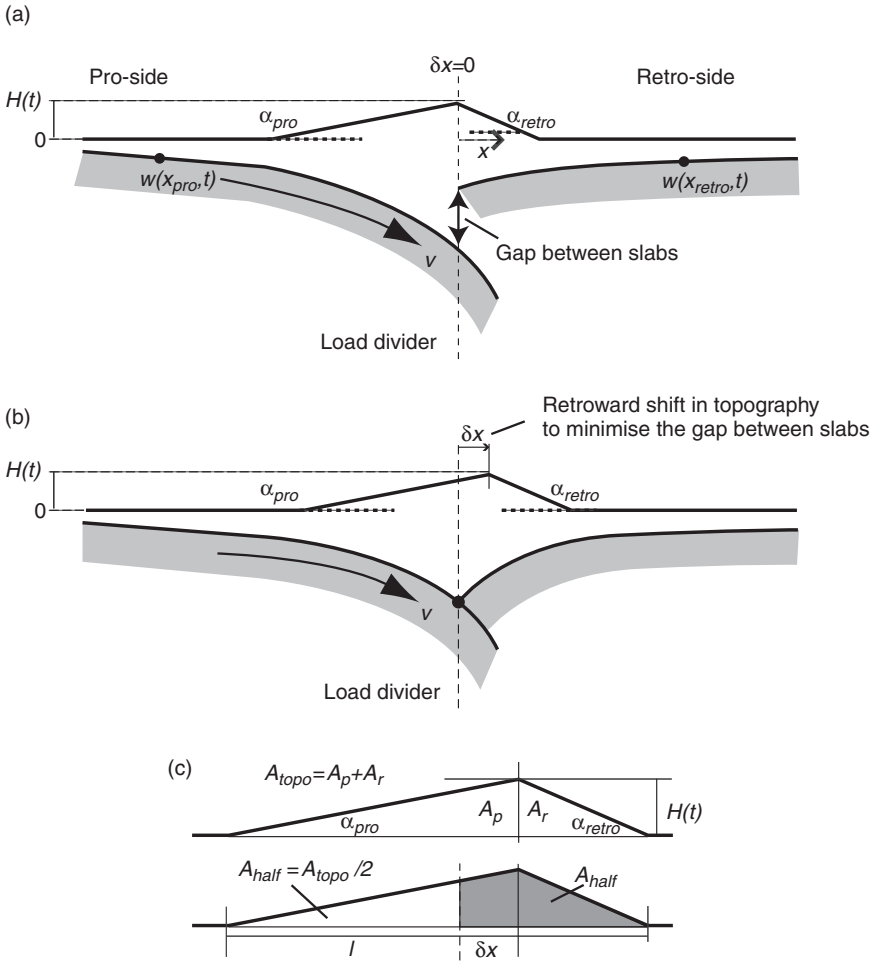

Fig. 2. End-member scenarios to balance the topographic load across the slabs. (a) The subducting slab supports the pro-wedge and the over-riding slab supports the retro-wedge. This leads to a discontinuity between the tips of the slabs. (b) The pro- and retro-wedges are shifted with respect to the slabs in order to ensure that the gap between the slabs is minimised. (c) The simplified model for topographic shift used in Appendix A.

 Basin Research, 10.1111/j.1365-2117.2008.00366.x

of zero deflection (i.e. approximately sea-level), however, all of our results are also directly applicable to under-filled basins.

The growth phase of the simulated mountain belt describes the period over which the wedge grows from nothing to a topographic maximum of 3 km elevation. By assuming a convergence rate and a thickness of material to be accreted into the mountain belt, h_0 we can determine the total amount of material that is accreted into the system after a period of time, t:

$$A_{\text{accreted}} = A_{\text{system}} + A_{\text{loss}} = vh_0t \tag{2}$$

Which implies that $A_{\text{accreted}} \geq A_{\text{system}}$. The loss of mass from the system represents the material that is transported out of the mountain belt – foreland basin system. It is trivial to incorporate transportation of material out of the system, however, this results in an non-unique solution which requires either calibration to a specific setting or full coupling to a surface process model. Because the aim of this paper is to define the first order signal, we take the unique end-member case where the basins are instantaneously filled and no material escapes the system such that $A_{\text{loss}} = 0$ and:

$$A_{\text{system}} = A_{\text{topo}} + A_{\text{fill}} = A_{\text{accreted}} = vh_0t \tag{3}$$

During the steady-state phase, A_{system} = constant and thus any additional material accreted is exactly balanced by material that is transported out of the system by erosion. In practice, A_{fill} is calculated from the current topographic distribution. Therefore to implement this model, at each model time-step we: (1) increment the topographic distribution $A_{\text{topo}} = A_{\text{topo}} + \Delta A$, (2) calculate the resulting increase in A_{fill}, and (3) calculate the age of the system using $t = (A_{\text{topo}} + A_{\text{fill}})/vh_0$.

Under this parameterisation, and choosing a value of $h_0 = 5.0$ km, material is accreted into the system at a rate of $\frac{dA}{dt} = vh_0 = 25\,\text{km}^2\,\text{Myr}^{-1}$. The sensitivity of the system to these choices of parameters is considered in the 'Summary and Discussion' section. As a rule of thumb for the Airy isostatic case, the deflected area is expected to be approximately five times the area of the topographic load. Thus, given that $A_{\text{topo}} = 275\,\text{km}^2$ and using the Airy approximation we can predicts the total duration required to grow the entire mountain belt system to the elevation of 3 km is $6\,A_{\text{topo}}/vh_0 \approx 66$ Myr. Further, the total topographic load at the end of the growth period is: $Q_{\text{topo}} = A_{\text{topo}}\,\rho_{\text{crust}}g = 7.28 \times 10^6$ MPa. To the first order, this approximation provides a reasonable estimate to the flexural case, which also depends on the flexural rigidity of the slabs, that can be measured directly from the simulation.

In the steady-state phase, we assume that the rate of accretion of new material is sustained and that time averaged influx of accreted material into the topographic wedge balances the erosional efflux of material out of the wedge such that the mean topography remains constant. The flexure model assumes that the fluctuations about this time average (Naylor & Sinclair, 2007) are negligible. As a result there is no further increase in the loading on the slabs once steady-state has been attained.

Flexure models

A flexure model provide a description for the shape of the slab which supports the mountain belt and its pro- and retro-foreland basins. The general flexure equation describing the deflection of an elastic plate assuming no horizontal compressional force and a hydrostatic restoring force is given by:

$$D\frac{d^4w(x,t)}{dx^4} + \Delta\rho g w(x,t) = q(x,t) \tag{4}$$

Where, $w(x, t)$ is the vertical deflection of point on the slab from the horizontal $z = 0$ datum at some time t, D is the flexural rigidity parameter and x is the horizontal distance from the free end of the slab. The second term represents the upward hydrostatic restoring force per unit area that results from the replacement of mantle rocks with crustal rocks in a layer of thickness w. Thus, $\Delta\rho = \rho_{\text{mantle}} - \rho_{\text{crustl}}$ and g is the acceleration due to gravity. We use this term to describe the instantaneous filling of the foreland basins. The applied load, $q(x, t)$ describes the time evolving vertical force per unit length at the position x, derived from the topography.

We assume that the system is supported on two semi-infinite plates which represent the subducting and overriding plates (Fig. 1b). Initially, the slabs are unloaded and flat, thus we ignore system specific pre-orogenic inherited stratigraphy.

We investigate two different end member solutions to Eqn. (4). Firstly, we use the end load solution to isolate the first-order role of the asymmetric tectonic boundary conditions in pro- and retro-foreland basin evolution. Secondly, we extend this model by coupling the basins together by appropriately partitioning the distributed topographic load. The distributed load scheme reduces to the endload model if the wedge angles are set to $\alpha_{\text{pro}} = \alpha_{\text{retro}} = 90^\circ$.

End load model

The end load model assumes that all of the topographic load, $q(x)$ can be reduced to a single line load, $Q(t)$ at the end of the slab such that:

$$q(0) = Q(t)$$
$$q(x \neq 0) = 0$$

The flexure of an elastic plate under the influence of an evolving end load (Turcotte & Schubert, 2001) is described by:

$$w(x,t) = \frac{\alpha^2 e^{-x/\alpha}}{2D}\left\{-M_0 \sin\frac{x}{\alpha} + (\alpha Q(t) + M_0)\cos\frac{x}{\alpha}\right\} \tag{5}$$

Where M_0 is a bending moment applied to the end of the slab. The bending moment affects the static shape of the slabs and the position of the pinchout point, however, our first-order conclusions are insensitive to its precise choice of value when it is taken to be a constant, so we set it to $M_0 = 0$. This reduces Eqn. (5) to:

$$w(x,t) = \frac{\alpha^3 e^{-x/\alpha}}{2D} Q(t) \cos\frac{x}{\alpha} \tag{6}$$

Where $D = ET_e^3/12(1-\upsilon^2)$ is the flexural rigidity with E the Young's modulus, T_e the effective thickness of the elastic plate and υ is Poisson's ratio. When the topography is modelled as an end-load, the fill between the slab and the $z = 0$ datum (the elevation of the stable cratonic plate) can be dealt with analytically via the density contrast in the flexural parameter

$$\alpha = \left(\frac{4D}{g(\rho_{mantle} - \rho_{fill})}\right)^{1/4} = 76\,km.$$

In order to focus on the first-order signal related to tectonic asymmetry and topographic form, we assume that both slabs have the same material properties $E = 70$ GPa, $T_e = 20$ km, $\upsilon = 0.25$ which are typical values for a young mountain belt (Allen & Allen, 2005); therefore $D = 5 \times 10^{22}$ Nm.

For the end load model we assume that the topographic load is distributed evenly across the pro- and retro-slabs. Thus the applied topographic load, to each slab, increases linearly from $Q(t=0) = 0$ to $Q_{final} = Q_{topo}/2 = 3.64 \times 10^6$ MPa. The total rate of accretion of material provides a loading rate of $\frac{dQ}{dt} = 0.5\rho_{crust} g \frac{dA}{dt} = 3.31 \times 10^5$ MPa Myr^{-1} for the whole system of topography and fill material.

A major limitation of the end load model is that it cannot simulate onlap driven by changing the distribution of topography as the pinchout point is analytically fixed. For this we require the distributed load model.

Distributed load model

The distributed load model takes into account the distribution of the thrust wedge topographic load. We apply a 1D solution to Eqn. (4) for a distributed load of arbitrary cross-section resting on a thin semi-infinite elastic plate that floats on a fluid substratum. The method approximates the continuous distribution, $q(x)$ by a distributed series of line loads. The impulsive response to each line load is summed to determine the total flexure of the slab (Garfunkel & Greiling, 2002).

For consistency with the end-load model, we again assume that the total area bounded by the flexed slab and the zero deflection datum is always filled, i.e. instantaneous filling of the basin to the surface of the stable cratonic plate on geological timescales. As for the end load model, we implement this using the density contrast term.

The geometrical relation between the topographic maximum and the slabs is not well constrained (Fig. 1b). Therefore, in deriving the coupled flexural history of the two basins, assumptions need to be made concerning the position of the topographic load with respect to the two slabs. We investigate two end-member scenarios that vary the position of the topographic maximum with respect to the underlying slabs; (i) allowing an open gap between the underthrust and over-riding slabs where each wedge is supported solely on its corresponding slab (Fig. 2a) and, (ii) the topography is shifted retrowards minimising the gap between the two flexed slabs (Fig. 2b).

The size of the gap between the slabs in the first scenario (Fig. 2a) is a function of the asymmetry of the distributed loads of the two thrust wedges, i.e. a more broadly distributed pro-wedge load vs. the narrower, but steeper retro-wedge load.

In order to test the plausibility of the scenario (ii), the retroward topographic shift minimising the gap between the slabs, we consider a simple analytic model that assumes the differential load is solely derived from the wedges (Fig. 2c). This allows us to test whether the magnitude of the retroward shift of topography lies within a geologically plausible range. In this analytic model, the horizontal separation between the ridge crest and the slab ends is a function of the height of the wedge and the wedge taper angles (Appendix A),

$$\delta x = H\left(\frac{1}{\tan\alpha_{pro}} - \sqrt{\frac{1}{2\tan\alpha_{pro}}\left(\frac{1}{\tan\alpha_{pro}} + \frac{1}{\tan\alpha_{retro}}\right)}\right) \tag{7}$$

For wedge angles in this study ($\alpha_{pro} = 1.5^\circ$, $\alpha_{retro} = 2.5^\circ$) the separation is given by $\delta x = 4.03H$. Thus, for our example of a mountain with mean topography at the highest point of $H = 3$ km, Eqn. (7) provides an initial estimate of the separation required between the convergence point of the underlying slabs and the surface drainage divide of $\sim$12.1 km, which is geologically reasonable.

Both of the scenarios predict a Bouguer gravity anomaly low on the pro-side of the topographic high, with the greatest offset occurring with the greatest asymmetries in wedge taper angles.

The case for the shifted topography is supported by (i) the fact that there is no mechanical reason to expect the pro- and retro-wedges to be solely supported on their respective slabs, (ii) computational models of orogenesis generally demonstrate a retro-ward shift in the topographic maximum with respect to the subduction point (Willett *et al.*, 1993; Naylor *et al.*, 2005).

RESULTS

In this section, we contrast the evolution of the pro- and retro-foreland basin model results in terms of stratigraphy, subsidence, basin geometry and rates of thrust deformation. Case 1, the end load model, provides the first order effects associated with the asymmetric tectonic boundary

conditions. Case 2, the distributed load model, highlights the important second-order effects associated with explicitly describing the thrust wedge as a distributed load. The simulated basins record only the foredeep depocenter (DeCelles & Giles, 1996) and does not consider sediment accumulated in wedge-top, forebulge or backbulge settings.

Case 1: end load model

Stratigraphic evolution

The stratigraphic evolution of the pro- and retro-foreland basins is summarised in Fig. 3.

The translation of the basin infill towards the subduction zone for the pro-foreland basin can be seen in both Fig. 3a and c, which leads to onlap at the basin margin. Because the basin fill is uniformly translated towards the orogen, the maximum residence time of any unit within the foredeep depocenter of the pro-foreland basin is given by the basin width divided by the convergence rate. The true width of the basin is poorly represented in the end-load model (Fig. 3) as the distributed topography is absent. In a foreland basin of width 60 km and regional convergence rate of 5 km Myr^{-1}, the turnover of the basin infill would be at least 12 Myr.

In contrast, the retro-foreland basin stores a complete record of the growth phase (Fig. 3b and d). A retro-foreland basin that is nearly full at the end of the growth phase has little space available for new sediment deposition once steady-state has been attained, with the majority of new material being transported across a basin-wide bypass surface. Thus, we expect the subsidence history of the retro-foreland basin to provide a good record of the entire growth phase, provided there was adequate sediment supply. As a consequence of the end load model, there is no onlap in the retro-side units at the basin margin (Fig. 3b and d).

Total subsidence histories

Predicted total subsidence histories of wells placed within the pro- and retro-foreland basins are plotted in Fig. 4. The retro-foreland basin shows constant, linear subsidence during the growth phase (Fig. 4a), with stratigraphic thickness increasing towards the orogen. During the steady-state phase, the subsidence histories that were locked in during the growth phase simply age with no further subsidence thus, a deceleration in subsidence through time. In contrast, the pro-foreland basin records a partial history of recent basin evolution. It shows the 'classic' acceleration of subsidence rates driven by basin translation following the flexural profile of the downgoing slab (Fig. 4b).

Consider the subsidence histories of the pro- and retro-foreland basins some time after steady-state has been attained (Fig. 4c). In this example, the lag between the last recorded subsidence in the retro-foreland basin and current time delimits the duration of the steady-state phase. There exists a contrast between short-duration, convex-upwards basin subsidence curves in pro-foreland basins and long-duration, concave-upward subsidence curves in

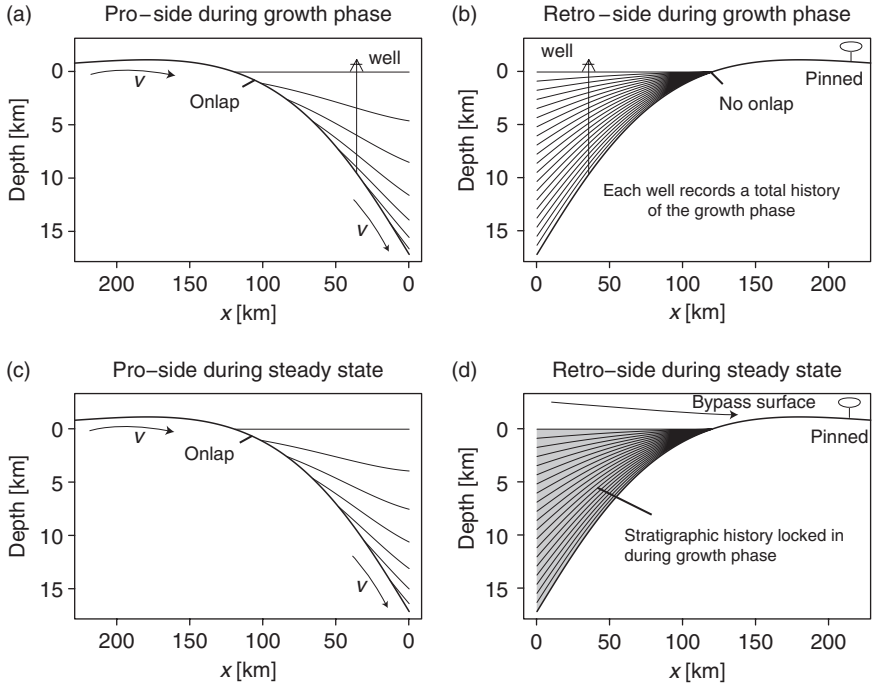

Fig. 3. Stratigraphic profiles for a pro- and retro-foreland basin modelled using an endload, applied at $x = 0$, during (a) and (b) the growth phase and (c) and (d) the steady-state phase. The stratigraphic horizons are spaced at 3.55 Myr intervals. The total duration for each run is 71 Myr. A well drilled in the retro-side basin records the entire growth phase. A well drilled in the pro-side only records a stratigraphic record related to the recent advection of the basin.

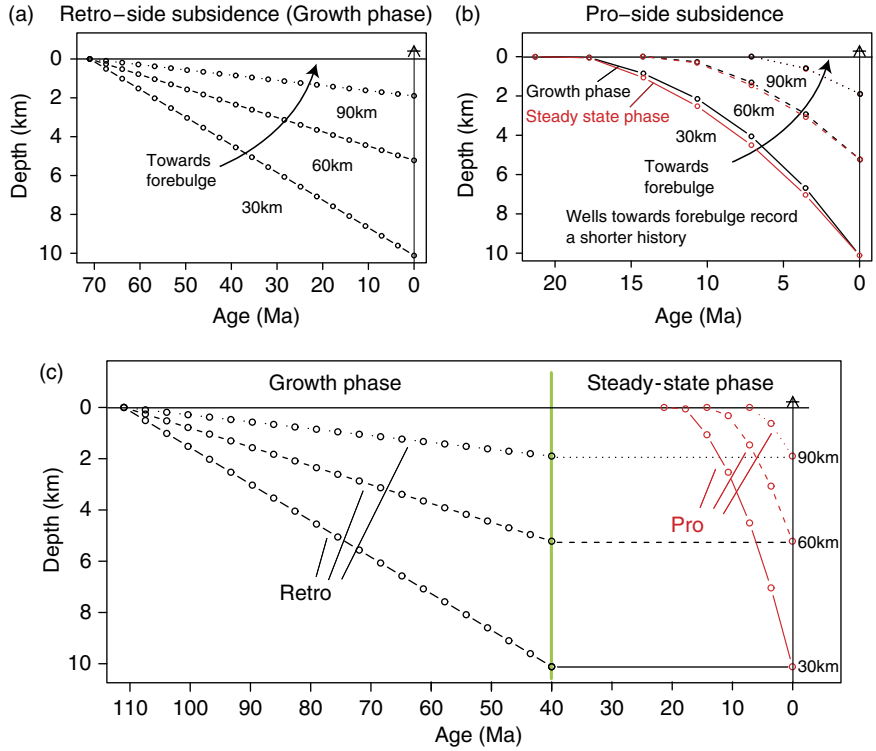

Fig. 4. Graphs of the subsidence histories recorded in wells located 30 km, 60 km and 90 km away from the endload. (a) The retro-side wells all record a complete history of the growth phase of the mountain-belt. There are no steady-state curves as no new accommodation space is created during the steady-state phase. (b) The pro-side wells only record a modern subset of the entire history as the oldest parts of the basin are being continually destroyed as they are accreted into the mountain belt. The growth phase shows greater acceleration of subsidence rates with due to the extra flexural component of subsidence. (c) A sample scenario of how the pro-foreland and retro-foreland subsidence curves relate to each other. The pro-side wells only record a partial history of the modern basin evolution. In contrast, the retro-side wells only record the growth phase and then steadily age with no further subsidence.

retro-foreland basins. A transition from the growth phase to a steady-state phase driven by the asymptotic convergence of uplift and erosion rates would be characterised by a more gradual and smoother retro-foreland subsidence curve than is suggested in Fig. 4c.

Case 2: distributed load model

The end load model demonstrates the first order signal derived from the asymmetric tectonic boundary conditions that require no assumptions about the topographic load distribution. We now use a distributed load model to investigate the second-order overprinting associated with the spatial distribution of mountain belt topography and the definition of the basin margin by the deformation front.

The cross-sectional evolution of the mountain belt for the open gap (Fig. 2a) and closed gap (Fig. 2b) loading schemes is shown in Fig. 5. The depth of the slab profiles is clearly sensitive to relatively subtle changes in the position of the topographic load. However, the basic basin evolution signal remains clear.

Onlap of cratonic margin

The position of both basin margins is now controlled by both the flexural parameter and the form of the distributed load (that defines the position of the deformation front). During the growth phase, the evolving distributed load introduces an extra flexural component that drives onlap in both the pro- and retro-foreland basins. This induced onlap by the encroachment of the thrust load for the retro-foreland basin is an important correction to the end load model. During growth of the system, the regional convergence drives the progressive accretion of new material into the thrust wedges, evolving the distributed load; at steady state, this accretion merely maintains a stable load distribution. Consequently, during growth, the time averaged rate of migration of the pro-foreland cratonic basin margin is greater than the regional convergence rate and equals it at steady state. In contrast the onlap rate of the cratonic margin of the retro-foreland basin is significantly less than the regional convergence rate during growth, and negligible at steady state.

Deformation fronts

The deformation fronts are defined to be the point where the wedge tips intersect the top of the basin succession (Fig. 5). As the wedges grow, the deformation fronts propagate out across the basins (red lines in Fig. 5 show the paleo-deformation front positions). Because the wedges must be the same height where they meet (at the load divider), the relative taper angles of the wedges controls the

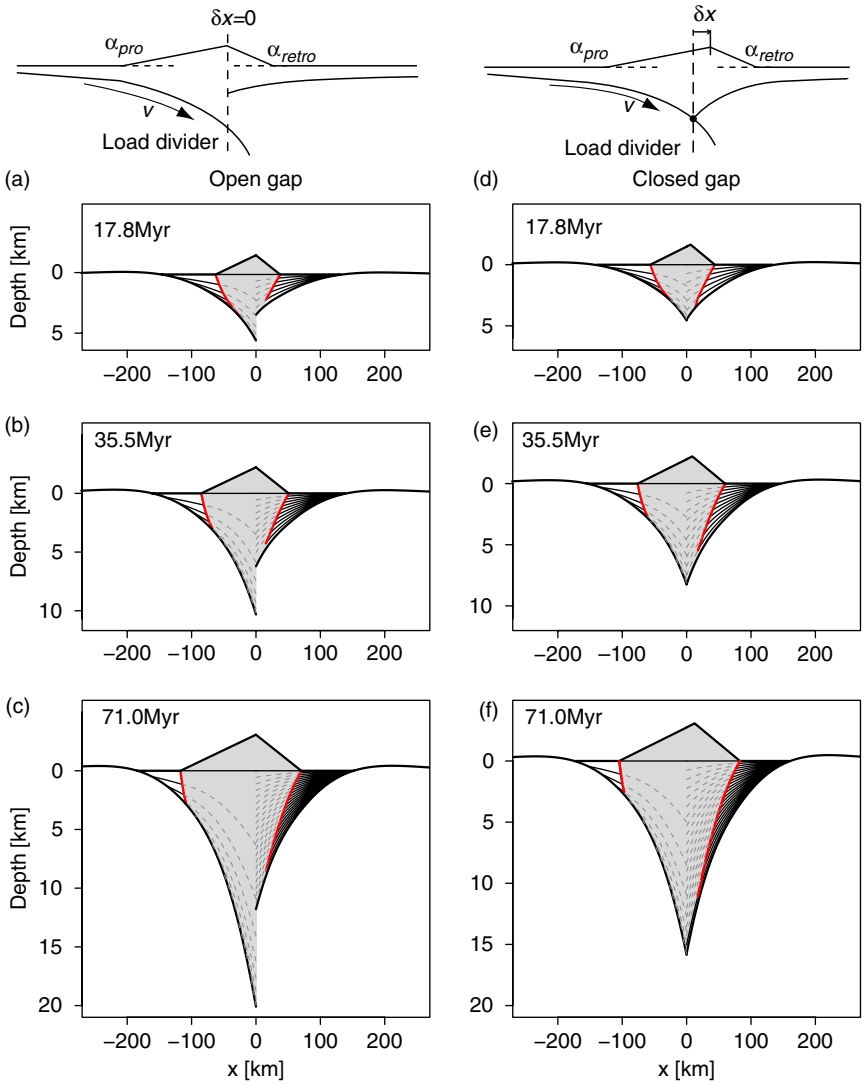

Fig. 5. Stratigraphic evolution of pro- and retro-foreland basins coupled by a topographic wedge load. (a–c) Show the time evolution for the open gap model where the pro-wedge is supported on the subducting slab and the retro-wedge is supported on the over-riding plate. (d–f) Show the time evolution for the closed gap model where the topographic load is shifted laterally in order to close the gap between the subducting and over-riding plates. The stratigraphic horizons are projected under the mountain belt as grey dashed lines to highlight the contrast between the basins; such stratigraphy is of course deformed as the basin is consumed at the deformation fronts. The evolution of the paleo-deformation front positions are shown in red (online).

relative rates at which the deformation fronts propagate out in order to accommodate the accretion of new material. As a kinematic consequence of how material is accreted into mountain belts, the mean surface slope angle of the retro-wedge is generally steeper than that of the pro-wedge (Willett *et al.*, 1993). Thus, geometrically, the topographic load of the retro-wedge is more compact than the pro-wedge load and more mass is stored in the pro-wedge than the retro-wedge. Further, the rate at which the deformation fronts propagate out across the basin are directly related to their taper angles. We can compare the rate at which the wedges grow using the cross-sectional areas of each wedge and noting that they must have the same height, H (Fig. 2c). The rate of propagation of each deformation front relative to the load divider is then the rate of change in the length of the base of the wedge,

$$\begin{aligned} \left(A^{\text{pro}}_{\text{topo}} = \frac{H^2}{2\tan\alpha_{\text{pro}}}\right) &> \left(A^{\text{retro}}_{\text{topo}} = \frac{H^2}{2\tan\alpha_{\text{retro}}}\right) \\ \left(v^{\text{pro}}_{\text{DF}} = \frac{\mathrm{d}H}{\mathrm{d}t}\frac{1}{\tan\alpha_{\text{pro}}}\right) &> \left(v^{\text{retro}}_{\text{DF}} = \frac{\mathrm{d}H}{\mathrm{d}t}\frac{1}{\tan\alpha_{\text{retro}}}\right) \end{aligned} \tag{8}$$

Thus, the rate at which the retro-wedge deformation front propagates out, v^{retro}_{DF} is slower than the pro-wedge deformation front v^{pro}_{DF} (Fig. 6a and b) provided $\alpha_{\text{retro}} > \alpha_{\text{pro}}$.

The rate at which material crosses the deformation fronts can be used to estimate the amounts of tectonic deformation, i.e. thrusting. The mean rate at which material is accreted at the pro-side deformation front is the sum of the rate at which the deformation front migrates out and

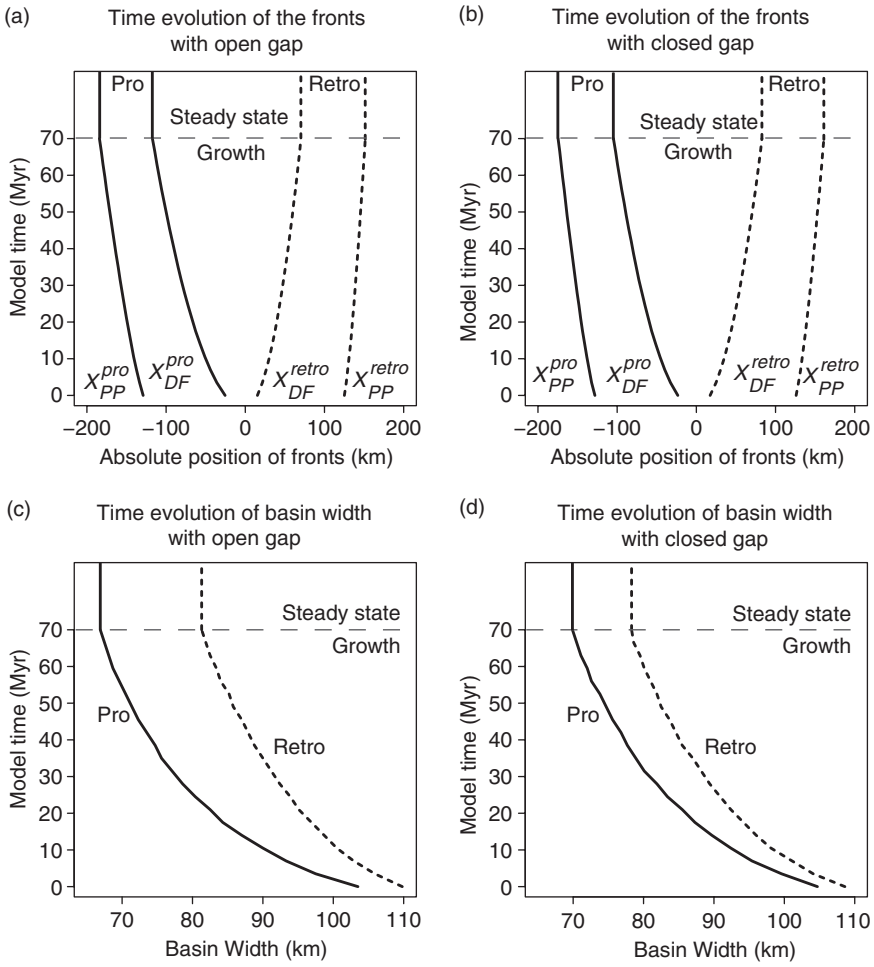

Fig. 6. Graphs showing the geometric evolution of the pro- and retro-foreland basin margins (solid lines for pro-foreland basin margins and dashed lines for the retro-foreland basin margins). (a and b) Show the absolute positions of the basin margins for the open gap and closed gap experiments, respectively. The outermost lines are the basin pinchout points, x_{PP} and the innermost lines are the deformation fronts, x_{DF}. (c and d) Show the resulting evolution of the basin widths. Notice that the retro-foreland basins (dashed lines) are wider than the pro-foreland basins (solid lines) and that closing the gap between the slabs minimises this difference.

the convergence rate at which the basin fill is translated towards the mountain belt. Because the retro-side basin fill is not translated and the retro-side deformation front propagates out at a slower rate than its counterpart on the pro-side; the rate of structural deformation (i.e. accretion) of the basin margin is significantly lower on the retro-side than the pro-side.

Basin width and depth

In contrast to the deformation fronts, the position of the basin margins is more strongly controlled by the flexural parameter than the topographic load, and so if we assume constant flexural rigidities, the retro-foreland basin is wider than the pro-foreland basin. This is a result of the degree to which the thrust wedge occupies the flexural deflection vs. the sediment infill; with lower taper thrust wedges, often characterised by a salt detachment, the wedge can propagate to occupy a large portion of the flexural depression (Ford, 2004), and so the foreland basins are relatively narrow. With steeper taper angles, as characterises retro-wedges, more of the flexural depression is filled with sediment rather than deformed wedge, hence the basins are wider (Fig. 6c and d). Because the retro-foreland basin is wider, so it is also deeper at the deformation front than the pro-foreland basin. This holds for both topographic load distribution scenarios (Fig. 5).

The width of both basins decreases as the mountain belt grows, primarily due to the deformation front propagating out faster than the pinchout point (Fig. 6). Because the rate at which the deformation fronts and basin margins propagate out decrease as the mountain belt grows, the width of the basins stabilises with time.

Chronostratigraphy of basin fill

Chronostratigraphic plots are key to understanding the temporal development of a basin, and are simply plotted as time against the distribution of sedimentation and erosion (Wheeler, 1964). In foreland basins, it is usual to plot the spatial development of the stratigraphy with reference to a stable cratonic foreland. However, when considering

 Basin Research, 10.1111/j.1365-2117.2008.00366.x

the synchronous development of two opposing foreland basins, it is interesting to note that these cannot be plotted on the same figure, as the cratonic forelands are moving relative to one another i.e. there is no fixed reference point. The reference frame for Fig. 6 is $x = 0$ the region where the slabs meet. The reference frame for the chronostratigraphic fronts in Fig. 7 is a fixed point on each of their respective plates. As the pro-foreland basin sits on the down going plate but is moving relative to it, the chronostratigraphic reference frame changes with respect to plate convergence rate as well as the growth of the foreland basin during the growth phase (for an expansion on this reference frame problem see Appendix B).

Given the difficulty of reference frames in these settings, we will consider the two basins separately, as if being studied on an individual basis. The contrasting character of the pro- and retro-chronostratigraphic plots (Fig. 7) can be summarised in terms of the temporal preservation of stratigraphy, and the rate of migration over the foreland. Pro-foreland basins only preserve the most recent record of basin development, the rest being accreted into the thrust belt. The age of the oldest sediments found at the bottom of the basin fill at the deformation front equates to the width of the basin times the rate of convergence. In contrast, retro-foreland basins preserve a much fuller history of mountain belt growth and steady state, as there is little destruction of the basin through accretion. However, the transition from growth to steady state should be recorded by a reduction in sediment accumulation rates, as there is no longer a tectonic driver of subsidence. There are only subtle differences between the open and closed gap experiments.

The onlap of the outer margin of a pro-foreland basin is driven by both the growth of the mountain belt, and the underthrusting of the plate at the convergence rate. Hence, during growth, the onlap rate combines these factors, but during steady state it should equate to the convergence rate (Fig. 7). In contrast, the progressive onlap of the retro-foreland basin can only be driven by the growth of the mountain belt, and so during steady-state onlap should cease.

EXAMPLES

Pro-foreland basins

The onlap of the cratonic margin of pro-foreland basins has been documented from the Palaeozoic Appalachian foreland basin (Quinlan & Beaumont, 1984; Tankard, 1986) the Cretaceous strata of the North Slope foreland basin, Alaska (Bird & Molenaar, 1992) and from numerous Tertiary examples such as the Pyrenees (Vergés *et al.*, 1998), Alps (Sinclair, 1997) and Taiwan (Lin *et al.*, 2003). As such it is a well known attribute of these basin types. As outlined in the model, such dramatic onlap is driven by the advection of the pro-foreland basin fill into the deforming thrust wedge. A further outcome of this is that these basin types typically only preserve a stratigraphic record of the more recent stages of orogenesis; the earlier basin fill being accreted into the thrust wedge, and commonly eroded. This is why there is a lack of stratigraphy older than ~16 Ma in the south Himalayan foreland basin of the Gangetic Plains when collision started ~50 Ma (Burbank *et al.*, 1996; Najman *et al.*, 2001). Similarly, there is only a partial preservation of the Eocene/Oligocene history of the North Alpine Foreland Basin in the folds and thrusts of the Helvetic domain of the Swiss Alps (Homewood *et al.*, 1986).

Subsidence histories of foreland basins in general are thought to be characterised by accelerating subsidence through time (Miall, 1995; Allen & Allen, 2005). We view this as a unique characteristic of pro-foreland basins supported by a range of examples including New Guinea/Timor Trough (Haddad & Watts, 1999), western Taiwan (Lin *et al.*, 2003), Ebro Basin, Pyrenees (Vergés *et al.*, 1998), and the North Alpine Foreland Basin (Allen *et al.*, 1986). As demonstrated in the modelling experiments, this pattern is dominated by subsidence induced by the progressive underthrusting of the slab beneath the mountain belt with a secondary component driven by any growth in the size of the topographic load. The former control does not occur in retro-foreland basins.

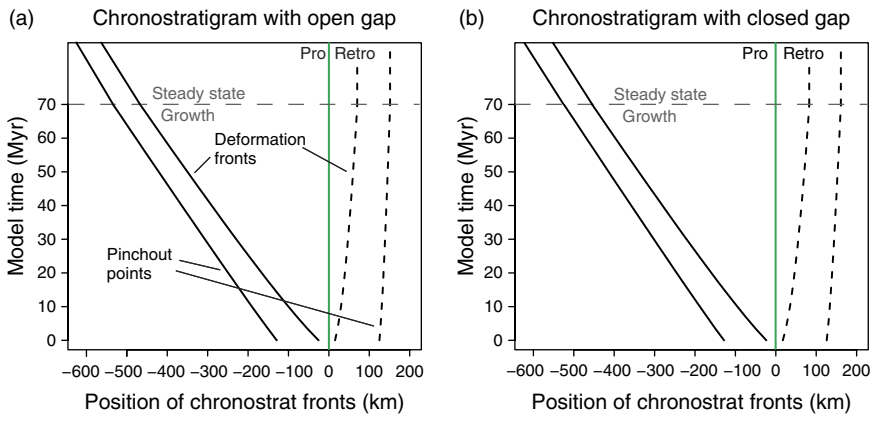

Fig. 7. Chronostratigraphic plots summarise the temporal preservation of stratigraphy, and the rate of basin migration over the foreland. The pro- and retro-chronostratigraphic plots are constructed relative to their respective stable cratons.

Retro-foreland foreland basins

Detailed documentation of retro-foreland basins is less common than for their pro-foreland counterparts. The Aquitaine Basin to the north of the Pyrenees in southern France (Fig. 8) is on the retro-side of the mountain belt (Sinclair *et al.*, 2005) and has been thoroughly documented due to the long history of hydrocarbon exploration and production (Bourrouilh *et al.*, 1995). In contrast to the pro-foreland basins described above, the Aquitaine Basin forms a wedge of sedimentary infill 4–6 km thick, that tapers over a distance of approximately 140 km away from the Pyrenees, and contains a full stratigraphic record of pre- and syn-orogenic sedimentation (Desegaulx *et al.*, 1991) (Fig. 8). The Upper Cretaceous to Oligocene units all thin onto the European craton with a wedge-shaped architecture that are vertically superimposed i.e. they exhibit little, if any, onlap. Additionally, the tectonic subsidence histories of the Aquitaine Basin (Fig. 8c) record a minor acceleration in subsidence at around the onset of Pyrenean orogenesis (~60 Ma), followed by a deceleration to zero since then (Desegaulx *et al.*, 1991). The pre-orogenic subsidence of the Aquitaine Basin records the remnant thermal subsidence to the thinned lithosphere. In contrast, the tectonic subsidence of a restored stratigraphic succession from the South Pyrenean Fold and thrust belt records a short-lived, accelerating record during early Eocene time. Additionally, in comparing the Aquitaine to the Ebro Basin (its pro-foreland counterpart), the amount of basin shortening is markedly different with approximately 60 km shortening of the Ebro Basin (Vergés, 1999) to < 10 km in the Aquitaine basin (Desegaulx & Brunet, 1990).

Another well documented example of a retro-foreland foreland basin is the South Westland Basin to the west of the Southern Alps, New Zealand (Kamp *et al.*, 1992; Sircombe & Kamp, 1998). This Pliocene basin is located immediately west of the steep retro-wedge dominated by the Alpine Fault (Beaumont *et al.*, 1996) and contains a full stratigraphic record of Southern Alps orogenesis. The shortening of the Australian plate adjacent to the basin is small (from 2 to 12 km), and is accommodated on steep basement faults rather than thin-skinned deformation; again attributes typical of retro-wedge deformation fronts. Tectonic subsidence within the basin accelerated at 5–6 Ma, and either remained steady or decelerated since that time as predicted above for retro-foreland basins. Similar examples of decelerating subsidence histories are documented for the Miocene history of the Tertiary Piedmont basin, which from Oligocene through early Miocene times was part of the western Po Basin compressional system (Carrapa *et al.*, 2003). Hence, this basin remnant records the retro-foreland basin of the southern

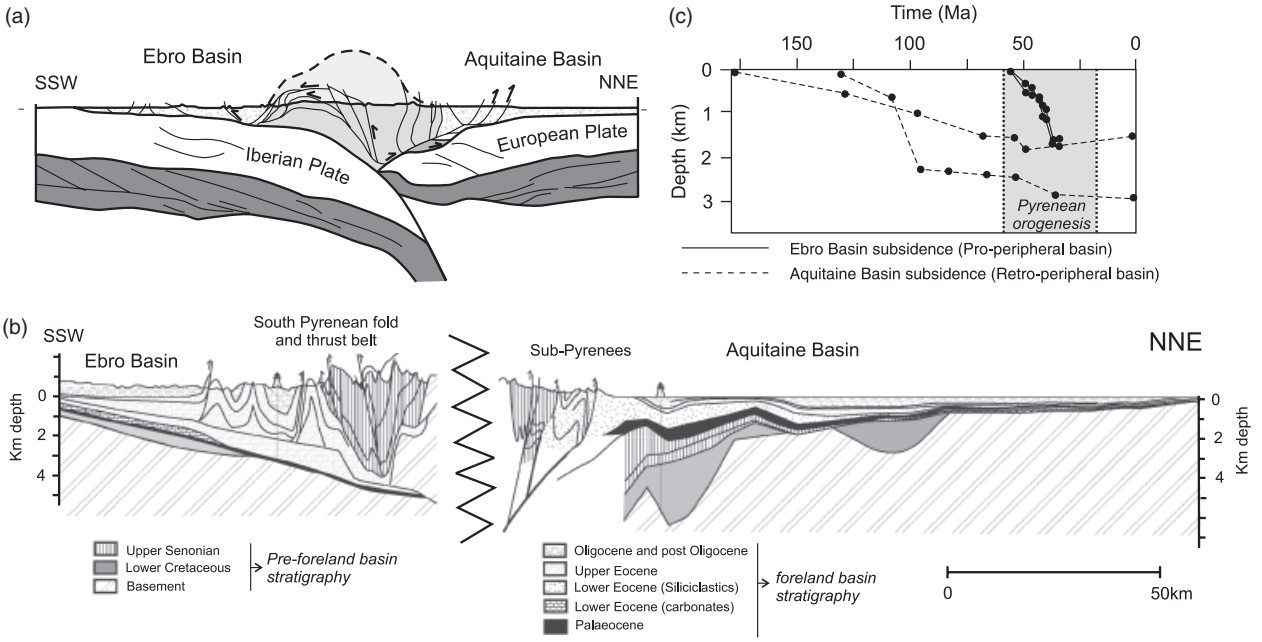

Fig. 8. The Pyrenees mountain belt as a type example of a system with a pro-foreland (Ebro Basin) and retro-foreland (Aquitaine Basin) foreland basin that can be compared in terms of their stratigraphic infill and tectonic subsidence histories. (a) Summary cross-section of the Pyrenean mountain belt formed by the Iberian plate of Spain subducting beneath the European Plate of south-western France. This section is constrained by the ECORS deep seismic section (Choukroune, 1989), other geophysical measurements (Pous *et al.*, 1995) and surface geology (Muñoz, 1992). (b) Close-up of the stratigraphy of the Ebro (Vergés, 1999) and Aquitaine Basins (Desegaulx *et al.*, 1991). (c) Subsidence plots from two wells located near to the deformation front in the Aquitaine Basin (Desegaulx & Brunet, 1990) and from structurally restored stratigraphic profiles from the central South Pyrenean fold and thrust belt (Vergés, 1999). Note that the Ebro Basin contains a limited section of stratigraphy dominated by Upper Eocene strata; the subsidence plots through this record a rapid phase of accelerating subsidence at this time. In contrast, the Aquitaine Basin contains a much broader chronostratigraphic range, and shows only minor tectonic subsidence during the early stages of orogenesis, but this decreases to zero. These contrasts match predictions made for pro-foreland vs. retro-foreland foreland basin development, respectively.

French Alps, although this is complicated by Apennine deformation and loading from the south.

The full stratigraphic record of orogenesis, the relatively insignificant record of progressive basin onlap, and the linear to decelerating subsidence histories of these basins fit the modelled predictions, and contrast with their pro-foreland counterparts.

SUMMARY AND DISCUSSION

While the chosen boundary conditions that determine slab behaviour beneath mountain belts are vital to understanding orogenesis, the predictions for the differentiation of pro- and retro-foreland basins require only an asymmetry of underthrusting and consequent thrust accretion.

The generic first-order signal is summarised in Fig. 9. A collisional mountain belt is generally bounded by two basins, a relatively mobile pro-basin above the subducting slab and a relatively stable retro-basin above the over-riding slab (Figs 8a and 9a). The rate of growth of the mountain belt is primarily controlled by the net rate of accretion of new material (Eqn. (2)). Thus the system will grow faster when accreting thicker material and for faster convergence rates. Varying the rate of accretion also has other implications because it controls the rate at which the pro-foreland basin fill is carried towards the mountain belt. Increasing the convergence rate increases the contrast between the pro- and retro-foreland basins; it increases the rate of tectonic deformation at the pro-deformation front which increasing the thickness of the accreted layer would not. However, increasing h promotes longer thrust sheets (Platt, 1988; Naylor & Sinclair, 2007). Varying accreted thickness can be taken into account by generalising Eqn. (2) to $A_{\text{accreted}} = \int vh(t)\mathrm{d}t$. Such changes in thickness may occur because of inherited rheology or a progressive transition from thin skinned to thick-skinned tectonics. The impact of increasing the thickness of the accreted layer is to increase the rate of accretion with time, delaying the convergence of uplift and erosion rates. However, such variations only transiently modify the behaviour we have documented in this paper rather than negating it.

The relative rates of migration of the deformation fronts relative to the load divide are purely a function of the wedge angles, assuming critical wedge theory. Rearranging Eqn. (8),

$$\frac{v_{DF}^{\text{pro}}}{v_{DF}^{\text{retro}}} = \frac{A^{\text{pro}}}{A^{\text{retro}}} = \frac{\tan\alpha_{\text{retro}}}{\tan\alpha_{\text{pro}}}$$

The pro- and retro- wedge angles, we chose are at the lower end of the range of observed angles. This affects the physical geometry, but it is the ratio of these angles that controls the relative asymmetry in the propagation rates. Increasing the wedge angles makes the mountain belt narrower, tending the system towards the endload model, and contains less mass for the same maximum height at the divide and is bounded by shallower basins.

Onlap is driven by both the outward propagation of the pinchout point by an increasingly distributed load and any relative motion between stable craton and the mountain belt that translates the basin fill; out of these two mechanisms it is the regional convergence that predominantly drives onlap. The mobile pro-foreland basin records onlapping stratigraphy and the oldest sediments in the basin can be found beneath the deformation front with an age approximated by the width of the basin divided by the regional convergence rate (Fig. 9b, Appendix B, eqn (B1)). Young sediments continue to onlap in the steady state phase while convergence is sustained. In contrast, the oldest sediments in the retro-foreland basin date from the initiation of growth of the mountain belt (eqn (B3)) and this basin records little onlap. As steady state is attained, the retro-foreland basin becomes filled and dormant with a bypass surface.

Owing to the long-term translation of the mobile pro-foreland basin towards the mountain belt at the far field convergence rate, the pro-foreland basin records accelerating subsidence (Fig. 9c). In contrast, the retro-basin records decelerating subsidence in the time period that relates to the transition from growth to steady state.

We can relate surface uplift to the increasing topographic mass by differentiating Eqn. (1),

$$\frac{\mathrm{d}A_{\text{topo}}}{\mathrm{d}t} = KH\frac{\mathrm{d}H}{\mathrm{d}t}$$

Where

$$K = \left(\frac{1}{\tan\alpha_{\text{pro}}} + \frac{1}{\tan\alpha_{\text{retro}}}\right).$$

From this, using the rate of accretion (2) and dropping the proportion of material that is accreted into the topography (which is approximately 1/6), we can rearrange for the surface uplift rate,

$$\frac{\mathrm{d}H}{\mathrm{d}t} \sim \frac{vh_0}{KH}$$

Increasing either wedge angle decreases K and increases the surface uplift rate required to accommodate a given influx of material. Further, this equation reinforces the relationship that the mean surface uplift rate will decrease as a mountain belts increase in size unless the rate of accretion of new material also increases. While this effect is not important for the first-order signal documented in this paper, it does become important when explicitly coupling such systems to a surface process model (e.g. Whipple & Meade, 2006) to investigate sediment sourcing and supply. Thus, the height of the mountain belt at steady state is also dependent upon the wedge angles (Dahlen & Suppe, 1988).

By studying the first-order effects that are distinguishable between pro- and retro-foreland basins we have made a number of assumptions in the modelling approach that need further qualification. The predicted evolution of the orogenic and cratonic basin margins for both basin types is depicted as the intercept of the deformation front and the

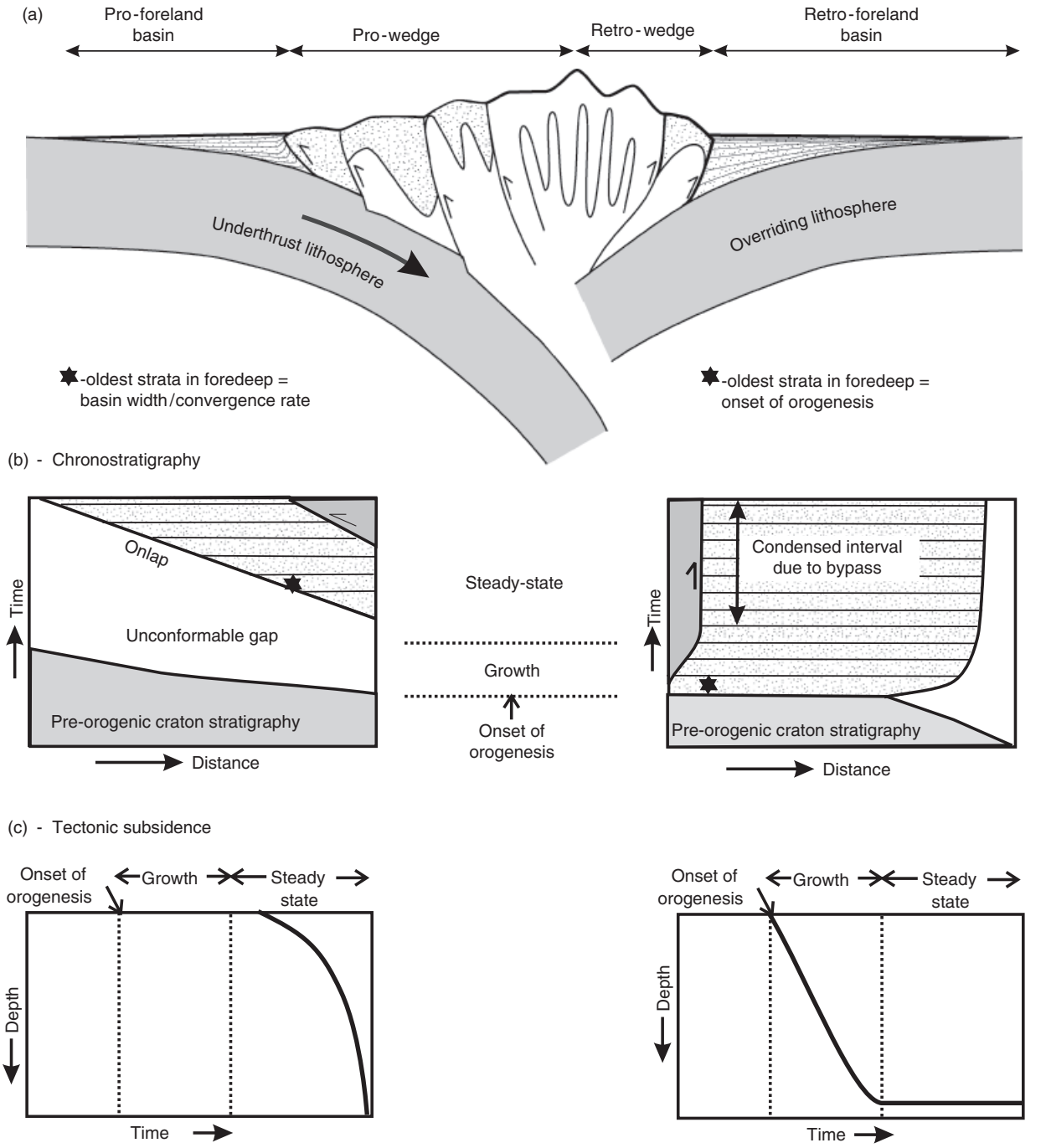

Fig. 9. Summary figure contrasting the basin characteristics of Pro-foreland (left-hand side) and Retro-foreland (right-hand side) foreland basins. (a) The Pro-foreland foreland basin exhibits dramatic basin onlap of the cratonic margin, at a rate greater or equal to the plate convergence rate dependent upon whether the thrust wedge is in a growth or steady-state phase, respectively; in contrast the Retro-foreland basin records little onlap except in the early stage of growth. This contrasting onlap pattern is clearly seen in the chronostratigraphic equivalent, (b) which also illustrates the relatively limited chronostratigraphic interval preserved in the pro-foreland basin relative to the retro-foreland basin. Note that the reference frame for both chronostratigraphic figures are their respective cratonic plates (cf. Appendix B and Fig. 10), and not an absolute frame. The degree to which foreland basin deposits are accreted and preserved in the thrust wedges also contrasts markedly due to the ongoing advection of the pro-foreland basin's succession into the pro-wedge, in contrast to the retro-foreland basin succession which will only be accreted during growth of the mountain belt. Hence, the oldest deposits preserved in the foredeep of the pro-foreland basin equal the width of the basin divided by the convergence rate. In contrast, the oldest strata preserved in the foredeep of the retro-foreland basin record the initiation of orogenesis. The tectonically driven subsidence of the two basins also contrasts, (c) The pro-foreland basin records accelerated subsidence over a relatively short interval of orogenesis. In contrast, the retro-foreland basin records the full history of the basin with initial uniform subsidence during growth of the mountain belt, and hence of the retro-thrust wedge, followed by zero subsidence during steady-state when the retro-wedge no longer accretes new material. During this latter stage, the retro-foreland basin record a condensed stratigraphic succession which is likely to be dominated by bypass of the sediment generated in the mountain belt and exported farther afield.

basin fill, and the stable craton and the basin fill, respectively. Naturally, the way in which sediment supply is modelled determines these parameters. For this exercise, we have assumed that all accommodation space in the basins are filled to a reference base-level (the $z = 0$ datum). Clearly, these geometries will differ for under or overfilled basin successions (Covey, 1986; Jordan, 1995). Consequently, it is essential that the nature of the stratigraphy used to approximate the cratonic basin margin is clearly documented in terms of the facies (Sinclair, 1997); i.e. whether they record coastal, deep-water or fully continental settings.

Critical to understanding output from numerical models is determining the role of the boundary conditions; in this case the laws that determine the behaviour of the downgoing tectonic slab and its impact on the growth of the doubly vergent thrust wedge. Understanding the nature of the coupling between the two slabs is a complicated issue and depends upon the nature and maturity of the orogen. For example, we applied the same flexural rigidity to both slabs, even though there is no requirement that the flexural rigidities should be the same. Such variations will modify the curvature of the slabs that bound the basins and change the topographic shift required to close the gap between the slabs. Because the shift in the topography did not have a major effect on the first order signal, we expect our conclusions to be robust to reasonable contrasts in elastic thickness between the two slabs.

In small, collisional orogens (e.g. Pyrenees, Olympics, Taiwan) with little evidence of crustal melting, the discussion of a physical coupling is justified, as the surface geology reveals discrete faulted contacts between rocks accreted from the downgoing slab vs. those accreted from the overlying slab (Muñoz, 1992; Willett *et al.*, 2003). Mountain belts with significant crustal melting of the root demonstrate the juxtaposition of crustal melt with mantle melt and the nature of the contact becomes less obvious. For very large orogens where their height is limited by the rheology of a flowing lower crust and mantle as recorded through volcanism (e.g. Himalaya/Tibet and Andes) the slabs are clearly decoupled. Examples such as the Southern Alps, New Zealand provide a case of strong thrust wedge asymmetry (Kamp & Tippett, 1993), but with continuous deformation of the mantle lithosphere, i.e. without a dominant subducting slab (Molnar *et al.*, 1999). Thus, while the separation of pro- and retro-wedges in settings such as the Southern Alps has been strongly advocated (Beaumont *et al.*, 1996), the deep structure that determines this asymmetry is debated.

WIDER IMPLICATIONS

Enhanced understanding of the coupling between the growth of mountain belts and the development of their associated foreland basins enables more sophisticated interpretation of foreland basin stratigraphy. Importantly, in order to gain insight into the growth phase of a mountain belt, it is clear that the best preserved records are at the base of the retro-foreland basin. It is possible to reconstruct this record from the pro-foreland basin, but only if the stratigraphy is preserved in the accreted thrust units of the pro-wedge of the mountain belt (e.g. Homewood *et al.*, 1986; Lihou & Allen, 1996). Similarly, it is the retro-foreland basin that should hold a record of the transition from growth of the mountain belt to steady-state; the subsidence histories should record this transition as a cessation of tectonic subsidence, and so the stratigraphy should reveal increased condensation. In contrast, the most recent history of orogenesis will always be preserved in the pro-foreland basin.

The distinction between linear basin subsidence induced by the growth of the thrust wedge and accelerating subsidence generated by the advection of the basin down and towards the mountain belt implies that subsidence histories may be inverted to distinguish these controls. The question of whether an overthrust plate has been actively subducted is usually investigated using geophysical imaging (Van der Voo *et al.*, 1999). We now consider basin subsidence records as a valuable additional tool to answering this question.

The recognition that peripheral foreland basins can be separated into two end-member models with distinct subsidence histories and stratigraphic architectures also has significant implications for hydrocarbon prospectivity. The subsidence history of a sedimentary basin is the primary control on the maturation history of hydrocarbons (Allen & Allen, 2005). Despite the presence of excellent structural traps on the edge of many foreland basins, source rocks are commonly 'overcooked' due to the rapid subsidence near the deformation front; this is particularly problematic for pro-foreland basins, with the notable exception of the Zagros thrust belt (Koop & Stoneley, 1982). The problem of overcooked source rocks is enhanced in post-orogenic settings when the basin is inverted in response to the reduction of the orogenic load. In examples such as the North Alpine Foreland Basin, the succession has been eroded and exhumed by over 1 km in the last 5 Myr in response to the cessation of deformation and increased erosion rates in the mountain belt (Cederbom *et al.*, 2004). Retro-foreland basins may also contain significant hydrocarbon reserves such as the Aquitaine Basin (Bourrouilh *et al.*, 1995). Hence, understanding the geodynamic context of a foreland basin in terms of it being a retro- or pro-foreland basin aids prediction of source rock maturation, and potentially reservoir architecture.

Finally, such a clear distinction between peripheral foreland basin types based on the asymmetry of the tectonic forcing raises the question of whether this has implications for understanding retro-arc foreland basins (Jordan, 1995). To a first order, the boundary conditions that characterise continent/continent collision appear similar to ocean/continent collision, i.e. the underthrusting or subduction of one lithosphere beneath another. Based on this, it is tempting to suggest that the model predictions for retro-foreland foreland basins should be similar to those for retro-arc foreland basins. However, there are some clear differences that may play a significant role in distinguishing the controls on these basin types. The marked density

contrast between oceanic and continental lithosphere is a strong driver of subduction leading to steeper subduction angles (Royden, 1993), enhanced melting (Pearce & Peate, 1995), and greater impact on mantle circulation and hence, dynamic topography (Burgess *et al*., 1997). Enhanced melting affects rheology, and hence the mechanical growth of the mountain belt (Willett *et al*., 1993), and dynamic subsidence due to mantle flow is superimposed on the isostatic signal, greatly enhancing the wavelength of subsidence of the retro-arc basin (Burgess *et al*., 1997). Therefore, we believe that retro-foreland and retro-arc foreland basins should be differentiated and that more work is needed to determine their contrasting characteristics.

CONCLUSIONS

In this paper, we have described how the asymmetrical forcing of orogenic systems by the underthrusting of one plate relative to the other results in contrasting foreland basins. Specifically,

Subsidence histories of pro-foreland basins comprise a linear component driven by thrust wedge growth, and an accelerating component driven by the advection of the basin towards the thrust wedge. In contrast, retro-foreland basins only subside in response to the growth of the thrust wedge, and hence are linear during the growth phase, and have no tectonic driver during steady-state. On a plot of subsidence through time, pro-foreland basin subsidence will be convex-upward, whereas retro-foreland basins are concave (Fig. 9c).

Pro-foreland basins are characterised by a basin fill that records only the recent history of the mountain belt; the recorded interval is given by the width of the basin divided by the plate convergence rate. In contrast, retro-foreland basins preserve the full stratigraphic record of mountain growth, but only a condensed record of steady-state development of a mountain belt (Fig. 9b).

Pro-foreland basins record basin onlap of the cratonic margin equal to the rate of plate convergence plus a component driven by outward growth of the thrust wedge. Retro-foreland basins record a relatively small amount of onlap driven solely by thrust wedge growth. During steady-state (i.e. with no growth), retro-foreland basins record little or no onlap, whereas pro-foreland basins record onlap equal to plate convergence rate (Fig. 9b).

These conclusions are supported by field examples. Classic examples of pro-foreland basins include the Appalachian foredeep, the Himalayan foredeep, the North Alpine Foreland Basin, the Ebro Basin (south Pyrenees) and the west Taiwan basin. Examples of retro-foreland basins include the South Westland Basin (New Zealand), The Po Basin (southern European Alps) and the Aquitaine Basin (north Pyrenees).

ACKNOWLEDGEMENTS

We would like to thank Brian Horton, Guy Simpson and an anonymous reviewer for constructive reviews and Ray Ingersoll for discussions on terminology. M.N. was funded by EPSRC grant GR/T11753/01 as part of the NANIA project.

REFERENCES

Allen, P.A. & Allen, J.R. (2005) *Basin Analysis*, 2nd edn. Blackwell Publishing, Oxford.

Allen, P.A., Homewood, P. & Williams, G.D., eds. (1986) *Foreland Basins: An Introduction*. Foreland Basins. International Association of Sedimentologists. Blackwell Scientific Publications, Oxford.

Beaumont, C. (1981) Foreland Basins. *Geophys. J. R. Astronom. Soc.*, **65**, 291–329.

Beaumont, C., Kamp, P.J.J., Hamilton, J. & Fullsack, P. (1996) The continental collision zone, South Island, New Zealand: comparison of geodynamical models and observations. *J. Geophys. Res.-Solid Earth*, **101**, 3333–3359.

Beaumont, C., Muñoz, J.A., Hamilton, J. & Fullsack, P. (2000) Factors controlling the alpine evolution of the Central Pyrenees inferred from a comparison of observations and geodynamical models. *J. Geophys. Res.-Solid Earth*, **105**, 8121–8145.

Bird, K.J. & Molenaar, M.C., eds. (1992) *The North Slope Foreland Basin, Alaska*. Foreland Basins and Fold Belts. American Association of Petroleum Geologists Memoirs, Tulsa.

Bourrouilh, R., Richert, J.P. & Zolnai, G. (1995) The North Pyrenean Aquitaine Basin, France – evolution and hydrocarbons. *AAPG Bull.*, **79**, 831–853.

Burbank, D.W., Beck, R.A. & Mulder, T., eds. (1996) *The Himalayan Foreland Basin*. The Tectonic Evolution of Asia Cambridge University Press.

Burgess, P.M., Gurnis, M. & Moresi, L. (1997) Formation of sequences in the cratonic interior of North America by interaction between mantle, eustatic, and stratigraphic processes. *Geol. Soc. Am. Bull.*, **109**, 1515–1535.

Carrapa, B., Bertotti, G. & Krijgsman, W. (2003) Subsidence, stress regime and rotation(s) of a tectonically active sedimentary basin within the Western Alpine Orogen: the tertiary Piedmont Basin (Alpine Domain, NW Italy). In: *Tracing Tectonic Deformation Using the Sedimentary Record* (Ed. by T. McCann & A. Saintot). **208**, 205–227. The Geological Society of London, London.

Cederbom, C.E., Sinclair, H.D., Schlunegger, F. & Rahn, M.K. (2004) Climate-induced rebound and exhumation of the European Alps. *Geology*, **32**(8), 709–712, doi: 10.1130/G20491.1.

Choukroune, P. (1989) The Ecors Pyrenean deep seismic profile reflection data and the overall structure of an Orogenic Belt. *Tectonics*, **8**, 23–39.

Covey, M. (1986) The evolution of Foreland Basins to steady state: evidence from the Western Taiwan Foreland Basin. In: *Foreland Basins* (Ed. by P.A. Allen & P. Homewood), *Spec. Publ. Int. Assoc. Sedimentol*. 77–90. Blackwell, Oxford.

Crampton, S.L. & Allen, P.A. (1995) Recognition of forebulge unconformities associated with early-stage Foreland Basin development – example from the North Alpine Foreland Basin. *AAPG Bull.*, **79**, 1495–1514.

Dahlen, F.A. & Suppe, J. (1988) Mechanics, growth and erosion of Mountain Belts. In: *Processes in Continental Lithospheric Deformation* (Ed. by S.P. Clark, B.C. Burchfiel & J. Suppe), *Geol. Soc. Amer. Spec. Pap* **218**, 161–178.

Dahlen, F.A., Suppe, J. & Davis, D. (1984) Mechanics of Fold-and-Thrust Belts and Accretionary Wedges – cohesive coulomb theory. *J. Geophys. Res.*, **89**, 87–101.

Davis, D., Suppe, J. & Dahlen, F.A. (1983) Mechanics of Fold-and-Thrust Belts and Accretionary Wedges. *J. Geophys. Res.*, **88**, 1153–1172.

DeCelles, P.G. & Giles, K.A. (1996) Foreland Basin systems. *Basin Res.*, **8**, 105–123, doi: 10.1046/j.1365-2117.1996.01491.x.

Desegaulx, P. & Brunet, M.F. (1990) Tectonic subsidence of the Aquitaine Basin since cretaceous times. *Bull. Soc. Geol. France*, **6**, 295–306.

Desegaulx, P., Kooi, H. & Cloetingh, S. (1991) Consequences of Foreland Basin development on thinned continental lithosphere – application to the Aquitaine Basin (SW France). *Earth Planet. Sci. Lett.*, **106**, 116–132.

Dickinson, W.R. (1974) Plate tectonics and sedimentation. In: *Tectonics and Sedimentation* (Ed. by W.R. Dickinson), *Spec. Publ.* **22**, 1–27. Society of Economic Paleontologists and Mineralogists, Los Angeles.

Flemings, P.B. & Jordan, T.E. (1989) A synthetic stratigraphic model of Foreland Basin development. *J. Geophys. Res.-Solid Earth Planets*, **94**, 3851–3866.

Ford, M. (2004) Depositional wedge tops: interaction between low basal friction external Orogenic wedges and flexural foreland basins. *Basin Res.*, **16**, 361–375, doi: 10.1111/j.1365-2117.2004.00236.x.

Garfunkel, Z. & Greiling, R.O. (2002) The implications of Foreland Basins for the causative tectonic loads. *EGU Stephan Mueller Spec. Publ. Ser.*, **1**, 3–16.

Haddad, D. & Watts, A.B. (1999) Subsidence history, gravity anomalies, and flexure of the Northeast Australian Margin in Papua New Guinea. *Tectonics*, **18**, 827–842.

Homewood, P., Allen, P.A. & Williams, G.D. (1986) Dynamics of the Molasse Basin of Western Switzerland. In: *Foreland Basins* (Ed. by P.A. Allen & P. Homewood). **8**, 199–219. International Association of Sedimentologists, Blackwell Scientific Publications, Oxford.

Johnson, D.D. & Beaumont, C. (1995) Preliminary results from a planform kinematic model of Orogen evolution, surface processes and the development of Clastic Foreland Basin Stratigraphy. In: *Stratigraphic Evolution of Foreland Basins* (Ed. by S.L. Dorobek & G.M. Ross), *Spec. Publ.* **52**, 3–24. Society of Economic Paleontologists and Mineralogists, Los Angeles.

Jordan, T.A. (1995) Retro-arc foreland and related basins. In: *Tectonics of Sedimentary Basins* (Ed. by C.J. Busby & R.V. Ingersoll), 331–363. Blackwell Science, Oxford.

Jordan, T.E. (1981) Thrust loads and Foreland Basin evolution, Cretaceous, Western United-States. *AAPG Bull.*, **65**, 2506–2520.

Kamp, P.J.J., Green, P.F. & Tippett, J.M. (1992) Tectonic architecture of the Mountain Front-Foreland Basin transition, South Island, New Zealand, assessed by fission track analysis. *Tectonics*, **11**, 98–113.

Kamp, P.J.J. & Tippett, J.M. (1993) Dynamics of Pacific Plate Crust in the South Island (New-Zealand) zone of oblique continent-continent convergence. *J. Geophys. Res.-Solid Earth*, **98**, 16105–16118.

Karner, G.D. & Watts, A.B. (1983) Gravity-anomalies and flexure of the lithosphere at mountain ranges. *J. Geophys. Res.*, **88**, 449–477.

Koop, W.J. & Stoneley, R. (1982) Subsidence history of the Middle-East Zagros Basin, Permian to recent. *Philos. Trans. R. Soc. Lond. Ser. A-Math. Phys. Eng. Sci.*, **305**, 149–168.

Lihou, J.C. & Allen, P.A. (1996) Importance of inherited rift margin structures in the Early North Alpine Foreland Basin, Switzerland. *Basin Res.*, **8**, 425–442.

Lin, A.T., Watts, A.B. & Hesselbo, S.P. (2003) Cenozoic stratigraphy and subsidence history of the South China Sea Margin in the Taiwan region. *Basin Res.*, **15**, 453–478, doi: 10.1046/j.1365-2117.2003.00215.x.

Miall, A.D. (1995) *Collision-Relate Foreland Basins*. Blackwell Science, Oxford.

Molnar, P., Anderson, H.J., Audoine, E., Eberhart-Phillips, D., Gledhill, K.R., Klosko, E.R., McEvilly, T.V., Okaya, D., Savage, M.K., Stern, T. & Wu, F.T. (1999) Continous deformation versus faulting through the continental lithosphere of New Zealand. *Science*, **286**, 516–519.

Muñoz, J.A. (1992) Evolution of a continental collision belt: ECORS-Pyrenees crustal balanced cross-section. In: *Thrust Tectonics* (Ed. by K. McClay). **17**, 235–246. Chapman & Hall, London.

Najman, Y., Pringle, M., Godin, L. & Oliver, G. (2001) Dating of the oldest continental sediments from the Himalayan Foreland Basin. *Nature*, **410**, 194–197, doi: 10.1038/35065577..

Naylor, M. & Sinclair, H.D. (2007) Punctuated thrust deformation in the context of doubly Vergent Thrust Wedges: implications for the localization of uplift and exhumation. *Geology*, **35**, 559–562, doi: 10.1130/G23448A.1.

Naylor, M., Sinclair, H.D., Willett, S.D. & Cowie, P.A. (2005) A discrete element model for Orogenesis and Accretionary Wedge growth. *J. Geophys. Res.*, **110**, doi: 10.1029/2003JB002940.

Pearce, J.A. & Peate, D.W. (1995) Tectonic implications of the composition of volcanic arc magmas. *Ann. Rev. Earth Planet. Sci.*, **23**, 251–285, doi: 10.1146/annurev.ea.23.050195.001343.

Platt, J.P. (1988) The mechanics of frontal imbrication – a lst-order analysis. *Geol. Rundschau*, **77**, 577–589.

Pous, J., Munoz, J.A., Ledo, J.J. & Liesa, M. (1995) Partial melting of subducted continental lower crust in the Pyrenees. *J. Geol. Soc.*, **152**, 217–220.

Quinlan, G.M. & Beaumont, C. (1984) Appalachian thrusting, lithospheric flexure, and the paleozoic stratigraphy of the eastern interior of North-America. *Can. J. Earth Sci.*, **21**, 973–996.

Royden, L.H. (1993) Evolution of retreating subduction boundaries formed during continental collision. *Tectonics*, **12**, 629–638.

Simpson, G.H.D. (2006) Modelling interactions between Fold-Thrust Belt deformation, Foreland flexure and surface mass transport. *Basin Res.*, **18**, 125–143, doi: 10.1111/j.1365-2117.2006.00287.x.

Sinclair, H.D. (1997) Tectonostratigraphic model for underfilled peripheral Foreland Basins: an Alpine perspective. *Geol. Soc. Am. Bull.*, **109**, 324–346.

Sinclair, H.D. & Allen, P.A. (1992) Vertical versus horizontal motions in the Alpine Orogenic Wedge: stratigraphic response in the Foreland Basin. *Basin Res.*, **4**, 215–232.

Sinclair, H.D., Coakley, B.J., Allen, P.A. & Watts, A.B. (1991) Simulation of Foreland Basin stratigraphy using a diffusion-model of Mountain Belt uplift and erosion – an example from the Central Alps, Switzerland. *Tectonics*, **10**, 599–620.

Sinclair, H.D., Gibson, M., Naylor, M. & Morris, R.G. (2005) Asymmetric growth of the Pyrenees revealed through measurement and modeling of Orogenic fluxes. *Am. J. Sci.*, **305**, 369–406.

Sircombe, K.N. & Kamp, P.J.J. (1998) The South Westland Basin: seismic stratigraphy, basin geometry and evolution of a Foreland Basin within the Southern Alps Collision Zone, New Zealand. *Tectonophysics*, **300**, 359–387.

Stockmal, G.S., Beaumont, C. & Boutilier, R. (1986) Geodynamic models of convergent margin tectonics – transition from rifted margin to Overthrust Belt and consequences for Foreland-Basin development. *AAPG Bull.*, **70**, 181–190.

Tankard, A.J. (1986) On the depositional response to thrusting and lithospheric flexure: examples from the Appalachian and Rocky Mountain Basins. In: *Foreland Basins* (Ed. by P.A. Allen & P. Homewood). **8**, 369–392. International Association of Sedimentologists, Blackwell Scientific Publications, Oxford.

Turcotte, D.L. & Schubert, G. (2001) Section 3–17. In: *Geodynamics* Ed. by 127. Cambridge, Cambridge University Press.

Van der Voo, R., Spakman, W. & Bijwaard, H. (1999) Tethyan subducted slabs under India. *Earth Planet. Sci. Lett.*, **171**, 7–20.

Vergés, J. (1999) Estudi Geologic Del Vessant Sud Del Pirineu Oriental I Central. In: *Evolucio Cinematica En 3d* (Ed. by Col-Leccio Monografies Tecniques, **7**, 194. Institut Cartografic de Catalunya, Barcelona.

Vergés, J., Marzo, M., Santaeulària, T., Serra-Kiel, J., Burbank, D.W., Muñoz, J.A. & Giménez-Montsant, J. (1998) Quantified vertical motions and tectonic evolution of the SE Pyrenean Foreland Basin. In: *Cenozoic Foreland Basins of Western Europe* (Ed. by A. Mascle, C. Puigdefàbregas, H.P. Luterbacher & M. Fernàndez), *Spec. Publ.* **134**, 107–134. Geological Society of London.

Wheeler, H.E. (1964) Baselevel, lithosphere surface, and time-stratigraphy. *Geol. Soc. Am. Bull.*, **75**, 599–610.

Whipple, K.X. & Meade, B.J. (2006) Orogen response to changes in climatic and tectonic forcing. *Earth Planet. Sci. Lett.*, **243**, 218–228, doi: 10.1016/j.epsl.2005.12.022.

Willett, S.D. (1992) Kinematics and dynamic growth and change of a Coulomb Wedge. In: *Thrust Tectonics* (Ed. by K. McClay), pp. 19–31. Chapman & Hall, London.

Willett, S.D., Beaumont, C. & Fullsack, P. (1993) Mechanical model for the tectonics of doubly Vergent Compressional Orogens. *Geology*, **21**, 371–374.

Willett, S.D. & Brandon, M.T. (2002) On steady states in Mountain Belts. *Geology*, **30**, 175–178, doi: 10.1130/0091-7613(2002)030⟨0175:OSSIMB⟩2.0.CO;2.

Willett, S.D., Fisher, D., Fuller, C., En-Chao, Y. & Lu, C.Y. (2003) Erosion rates and orogenic-wedge kinematics in Taiwan inferred from fission-track thermochronometry. *Geology*, **31**, 945–948, doi: 10.1130/G19702.1.

Manuscript received 24 September 2007; Manuscript accepted 7 May 2008.

APPENDIX A

The basis for this analysis is illustrated in Fig. 2c. This first order analysis assumes that the gap between the slabs is minimised when the topography is shifted such that half of the total topographic area is supported by each slab.

Given the total topographic area, we can calculate half of that value:

$$A_{\text{topo}} = \frac{H^2}{2\tan\alpha_{\text{pro}}} + \frac{H^2}{2\tan\alpha_{\text{retro}}}$$

$$A_{\text{half}} = A_{\text{topo}}/2 = \frac{H^2}{4}\left(\frac{1}{\tan\alpha_{\text{pro}}} + \frac{1}{\tan\alpha_{\text{retro}}}\right)$$

Because the pro-wedge has a larger area than the retro-wedge, we equate half of the total area to a triangle with base length l and slope angle α_{pro}:

$$A_{\text{half}} = \frac{l^2\tan\alpha_{\text{pro}}}{2}$$

$$\Rightarrow l = \sqrt{\frac{2A_{\text{half}}}{\tan\alpha_{\text{pro}}}} = H\sqrt{\frac{1}{2\tan\alpha_{\text{pro}}}\left(\frac{1}{\tan\alpha_{\text{pro}}} + \frac{1}{\tan\alpha_{\text{retro}}}\right)}$$

The total width of the pro-wedge is $L = H/\tan\alpha_{\text{pro}}$, which is greater than l. Therefore the approximate horizontal separation δx between the ridge crest and the contact between the slabs, to minimise the gap between the slabs, is given by:

$$\delta x = L - l = \frac{H}{\tan\alpha_{\text{pro}}} - l$$

$$= H\left(\frac{1}{\tan\alpha_{\text{pro}}} - \sqrt{\frac{1}{2\tan\alpha_{\text{pro}}}\left(\frac{1}{\tan\alpha_{\text{pro}}} + \frac{1}{\tan\alpha_{\text{retro}}}\right)}\right)$$

APPENDIX B: FRAMES OF REFERENCE

The position of the pro-deformation front and pro-foreland basin margin in a chronostratigraphic diagram (black lines in Fig. 10) are different from those in the absolute frame of reference (red lines in Fig. 10). In fact, the positions of the pro-side chronostratigraphic fronts, $X^{\text{pro}}_{\text{Chronostrat}}$ are in a different frame of reference to the retro-side chronostratigraphic fronts, $X^{\text{retro}}_{\text{Chronostrat}}$. This is because the pro-side chronostratigraphic fronts are

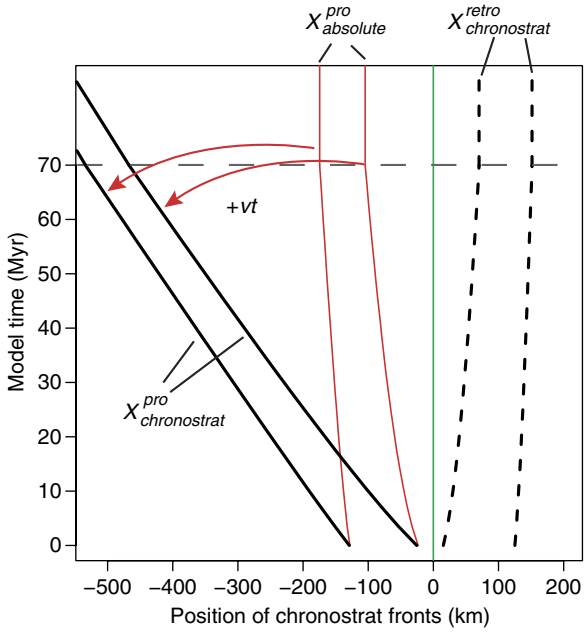

Fig. 10. Demonstration of how the evolution of the basin margins as measured relative to a point on the stable craton can be transformed into a stationary frame of reference, relative to the centre of the mountain belt. The black lines show the position of the pro- and retro-deformation fronts and basin margins relative to their respective stable cratons, as measured by the stratigraphic record. The red lines show the position of the pro-side deformation front and basin margin relative to the core of the mountain belt. The conversion between the two requires knowledge of the total amount of shortening that has occurred between the pro-side craton and the mountain belt. See online version for colour figure.

measured with respect to a stable point on the pro-side craton while the retro-side chronostratigraphic fronts are measured with respect to a stable point on the retro-side craton. Because the pro-side craton is moving towards the retro-side craton at the regional convergence rate, the pro- and retro-chronostratigraphic diagrams must be in a different frame of reference. This is not the case in the absolute frame of reference, $X^{\text{pro}}_{\text{Absolute}}$ and $X^{\text{retro}}_{\text{Absolute}}$. Thus the mapping between the absolute frame and the chronostratigraphic frame is:

$$\begin{aligned} X^{\text{pro}}_{\text{Chronostrat}}(t) &= X^{\text{pro}}_{\text{Absolute}}(t) + vt \\ X^{\text{retro}}_{\text{Chronostrat}}(t) &= X^{\text{retro}}_{\text{Absolute}}(t) \end{aligned} \quad \text{(B1)}$$

Assuming that the rate at which the position of the deformation front, X_{DF} and basin margin pinchout point, X_M migrate are small with respect to the regional convergence rate, the stratigraphic duration of the pro-foreland basin record and the depositional age of the sediments at the bottom of a well at its deformation front are coincident and given by the distance between its basin margins divided by the convergence rate:

$$\tau_{\text{pro-basin}} \approx \frac{X_M - X_{DF}}{v} \quad \text{(B2)}$$

The age of the deepest sediments youngs towards the cratonic basin margin, reflected in the onlapping stratigraphy. In contrast, the duration of the record held in the retro-foreland basin is given by the duration of the growth phase which can be calculated by determining how long it took to grow the entire system to steady-state:

$$\tau_{\text{retro-basin}} \approx \frac{A_{\text{system}}}{vh_0} \quad \text{(B3)}$$

The age of the deepest sediments is given by the total duration because growth of the system started. These oldest sediments are spread across the entire retro-foreland basin, except in the small region of onlap associated with the migration of the pinchout point.

Parameter List

Flexural parameters

$E = 70\,\text{GPa}$	Young's modulus
$\upsilon = 0.25$	Poisson's ratio
$T_e = 20\,\text{km}$	Elastic thickness
	Flexural rigidity

$D = ET_e^3/12(1-\upsilon^2) = 5 \times 10^{22}\,\text{Nm}$

$g = 9.8\,\text{m s}^{-2}$	Acceleration due to gravity
$\rho_{\text{mantle}} = 3300\,\text{kg m}^{-3}$	Mantle density
$\rho_{\text{crust}} = 2700\,\text{kg m}^{-3}$	Crustal density
$\Delta\rho = \rho_{\text{mantle}} - \rho_{\text{crust}} = 600\,\text{kg m}^{-3}$	Density contrast
$\alpha = \left(\frac{4D}{g(\rho_{\text{mantle}} - \rho_{\text{filli}})}\right)^{1/4} = 76\,\text{km}$	Flexural parameter
$M_0 = 0$	Applied end bending moment
$w(x, t)$	Deflection of slab
$q(x)$	Distributed load

Tectonic boundary conditions

$v = 5.0\,\text{mm yr}^{-1}$	Regional convergence rate
$h_0 = 5.0\,\text{km}$	Accreted layer thickness

(Implicit assumption that the retro-side layer thickness is the same.)

Wedge and basin geometry

$\alpha_{\text{pro}} = 1.5^\circ$	The angle which the pro-wedges make wrt to the horizontal
$\alpha_{\text{retro}} = 2.5^\circ$	The angle which the retro-wedges make wrt to the horizontal
$\rho_{\text{topo}} = \rho_{\text{fill}} = \rho_{\text{crust}} = 2700\,\text{kg m}^{-3}$	Assume that the density of the upper crustal material is invariant.
$H_{\text{max}} = 3\,\text{km}$	Height of drainage divide at end of the growth phase
$A_{\text{topo}} = \frac{H^2}{2\tan\alpha_{\text{pro}}} + \frac{H^2}{2\tan\alpha_{\text{retro}}}$	Area under topographic wedge
A_{fill}	Area above slabs and beneath zero deflection datum, comprises foreland basins and root of mountain belt
$A_{\text{system}} = A_{\text{topo}} + A_{\text{fill}}$	Total cross-sectional area of the simulated mountain belt
A_{accreted}	The total amount of material accreted from the underthrust plate
X_{M}	Position of basin margin
X_{DF}	Position of deformation front
$\tau_{\text{pro-basin}}$	Duration of pro-foreland basin record
$\tau_{\text{retro-basin}}$	Duration of retro-foreland basin record

